ORIGINAL ARTICLE

JIMD | SSIEM | WILEY

Use of pure recombinant human enzymes to assess the disease-causing potential of missense mutations in urea cycle disorders, applied to *N*-acetylglutamate synthase deficiency

Nadine Gougeard[1,2] | Enea Sancho-Vaello[1] |
M. Leonor Fernández-Murga[1] | Borja Martínez-Sinisterra[1] |
Badr Loukili-Hassani[1] | Johannes Häberle[3] | Clara Marco-Marín[1,2] |
Vicente Rubio[1,2]

[1]Instituto de Biomedicina de Valencia, IBV-CSIC, Valencia, Spain

[2]Group 739, Centro de Investigación Biomédica en Red de Enfermedades Raras, (CIBERER-ISCIII) at the IBV-CSIC, Valencia, Spain

[3]University Children's Hospital Zurich and Children's Research Centre, Zurich, Switzerland

Correspondence
Clara Marco-Marín and Vicente Rubio, Instituto de Biomedicina de Valencia (IBV-CSIC), Jaime Roig 11, Valencia 46010, Spain.
Email: cmarco@ibv.csic.es and rubio@ibv.csic.es

Present addresses
Enea Sancho-Vaello, Department of Biochemistry and Molecular Biology, Universitat Autònoma de Barcelona, Cerdanyola del Vallés, Spain; and M. Leonor Fernández-Murga, Clinical and Molecular Oncology Laboratory, Hospital Arnau de Vilanova-Liria, FISABIO, Valencia, Spain.

Funding information
Fundación Ramón Areces, Grant/Award Number: CIVP20A6610; Ministerio de Economía y Competitividad, Grant/Award Number: BFU2017-84264-P; Schweizerischer Nationalfonds zur

Abstract

N-acetylglutamate synthase (NAGS) makes acetylglutamate, the essential activator of the first, regulatory enzyme of the urea cycle, carbamoyl phosphate synthetase 1 (CPS1). NAGS deficiency (NAGSD) and CPS1 deficiency (CPS1D) present identical phenotypes. However, they must be distinguished, because NAGSD is cured by substitutive therapy with the *N*-acetyl-L-glutamate analogue *N*-carbamyl-L-glutamate, while curative therapy of CPS1D requires liver transplantation. Since their differentiation is done genetically, it is important to ascertain the disease-causing potential of *CPS1* and *NAGS* genetic variants. With this goal, we previously carried out site-directed mutagenesis studies with pure recombinant human CPS1. We could not do the same with human NAGS (HuNAGS) because of enzyme instability, leading to our prior utilization of a bacterial NAGS as an imperfect surrogate of HuNAGS. We now use genuine HuNAGS, stabilized as a chimera of its conserved domain (cHuNAGS) with the maltose binding protein (MBP), and produced in *Escherichia coli*. MBP-cHuNAGS linker cleavage allowed assessment of the enzymatic properties and thermal stability of cHuNAGS, either wild-type or hosting each one of

We dedicate this article to the late (August 04, 2022) Santiago Grisolia, discoverer of the activation by *N*-carbamylglutamate of citrulline synthesis by liver mitochondria, and maker (together with V.R.) of the *N*-carbamylglutamate given to the first reported patient of NAGS deficiency.

Nadine Gougeard and Enea Sancho-Vaello are co-first authors.

23 nonsynonymous single-base changes found in NAGSD patients. For all but one change, disease causation was accounted by the enzymatic alterations identified, including, depending on the variant, loss of arginine activation, increased $K_m^{Glutamate}$, active site inactivation, decreased thermal stability, and protein misfolding. Our present approach outperforms experimental in vitro use of bacterial NAGS or in silico utilization of prediction servers (including AlphaMissense), illustrating with HuNAGS the value for UCDs of using recombinant enzymes for assessing disease-causation and molecular pathogenesis, and for therapeutic guidance.

KEYWORDS

inborn errors, maltose binding protein, MBP-NAGS chimera, NAGS, NAGS deficiency, site-directed mutagenesis, urea cycle

1 | INTRODUCTION

We previously showed that only a fraction of the possible single-amino acid changes in the urea cycle (UC) enzyme ornithine transcarbamylase (OTC; EC 2.1.3.3) cause OTC deficiency (OTCD; MIM no. 311250).[1] This seems to be the general case among inborn metabolic errors. Thus, discrimination between disease-causing and trivial variants is essential.[2] In silico pathogenicity prediction servers are helpful but are not entirely reliable.[3] Sounder proof of disease causality can be obtained by site-directed mutagenesis of recombinantly expressed target proteins, generally focusing on patient-identified variants (see e.g.,[4–14]). Recently introduced deep mutagenesis approaches use massive parallel assays,[15] although this costly approach is in an early stage (discussed in Ref. [16]), having been used thus far for a single UC disorder (UCD), OTCD.[17]

Few experimental studies[11–14] have investigated disease causality of patient-found variants in the UCD *N*-acetylglutamate synthase (NAGS; EC 2.3.1.1) deficiency (NAGSD; MIM no. 237310), although many *NAGS* gene variants of uncertain significance have been identified in the population (https://gnomad.broadinstitute.org/gene/ENSG00000161653?dataset=gnomad_r4). The scarcity of experimental studies may reflect the rarity of NAGSD,[18] as well as technical difficulties due to intrinsic instability/tendency to aggregate of eukaryotic NAGSs (well documented for rodent and yeast NAGSs[19,20]). It is particularly important to ascertain the disease causality of patient-found human NAGS (HuNAGS) variants. In humans, NAGS sole function[21,22] is to produce *N*-acetyl-L-glutamate (NAG), the essential allosteric activator of the first and controlling enzyme of the UC, carbamoyl phosphate synthetase 1 (CPS1; EC6.3.4.16).[23,24] Thus, NAGSD and CPS1 deficiency (CPS1D; MIM no. 237300)

are phenotypically identical and have no reliable differential biomarkers. Their differentiation, now based on gene sequencing[25] (see an example of misdiagnosis corrected by genetics in Refs. [14,26]), is important, since NAGSD, by having substitutive therapy with the NAG analogue *N*-carbamyl-L-glutamate (NCG),[27,28] does not require liver transplantation for cure, unlike CPS1D and other UCDs.[29] Some CPS1D patients can also benefit from NCG therapy. Their response, generally partial,[30,31] limits the reliability of testing the effect of NCG administration on hyperammonemia as a way to differentiate CPS1D and NAGSD.

We previously carried out site-directed mutagenesis studies in human CPS1 to investigate experimentally the disease causality of single amino acid replacements found in CPS1D.[7,32,33] However, we could not do the same with HuNAGS, due to enzyme instability. We had to rely on the utilization of a bacterial NAGS, used as a surrogate of HuNAGS.[14] Now we circumvent the HuNAGS instability problem by expressing from a plasmid, in *Escherichia coli*, the conserved region[11,12,34] of HuNAGS (cHuNAGS, Figure 1A) as part of a chimera with a His6-tagged maltose binding protein (MBP; Figure 1B). By releasing the cHuNAGS from the chimera by cleavage of the MBP-cHuNAGS linker with PreScission protease, and then by carrying out functional and stability assays of separate cHuNAGS, we clarify here the effects on HuNAGS of 23 nonsynonymous single nucleotide changes (including a 37-residue C-terminal truncation) identified in NAGSD patients. Previously, we had subjected these changes to in silico analysis, and, when feasible, to experimental site-directed mutagenesis studies using *Pseudomonas aeruginosa* NAGS (PaNAGS) as a model of HuNAGS.[14]

We prove here the superiority of the present approach over both our earlier approaches[14] and the novel AlphaMissense tool,[16] which uses artificial intelligence. Our
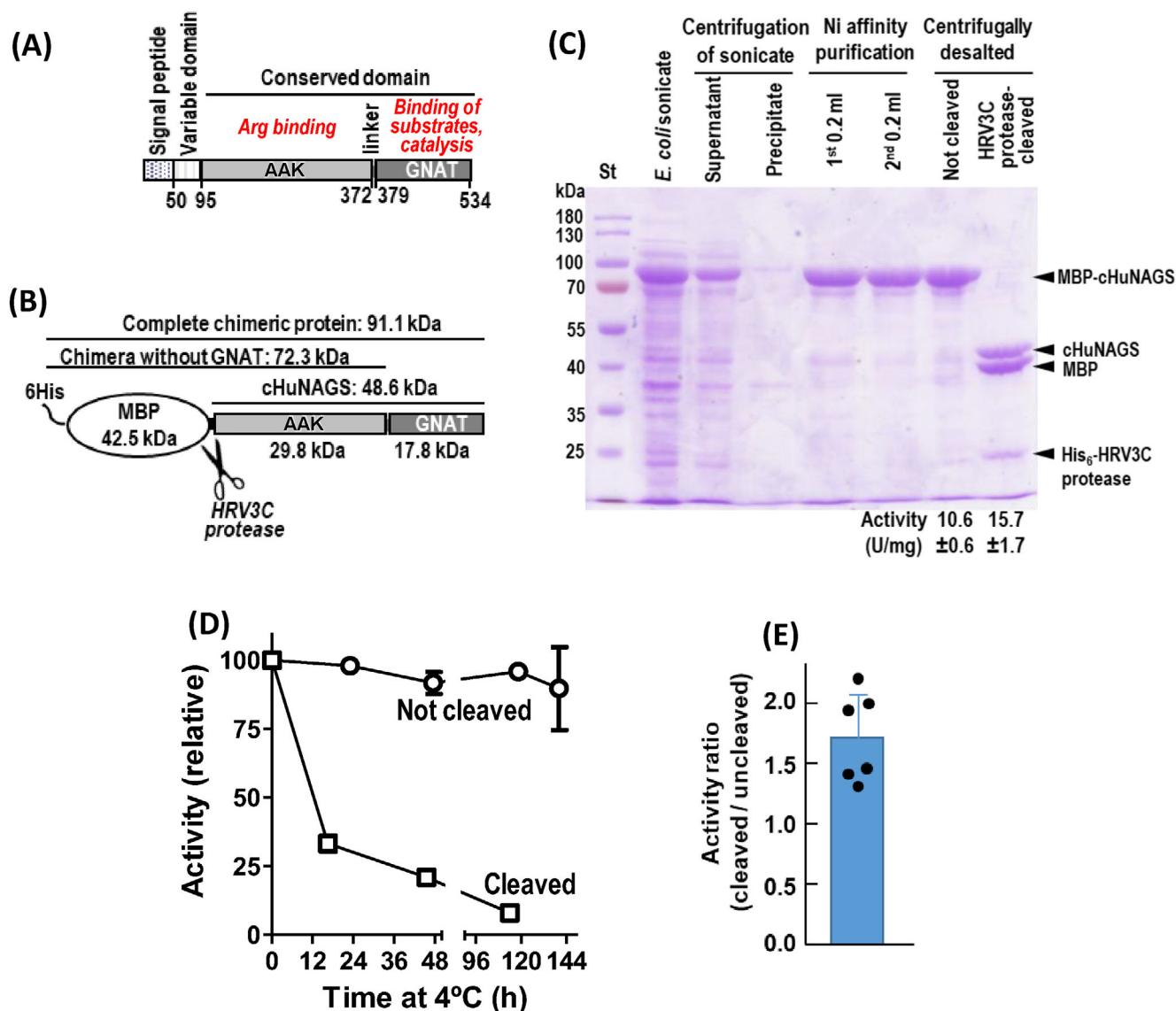
FIGURE 1 cHuNAGS production, purification, activity, and properties before and after cleavage of the maltose binding protein (MBP)-cHuNAGS linker. Enzyme activity was determined in the standard assay. Results are means ± SEM for at least two assays. (A) Linear scheme of human *N*-acetylglutamate synthase (NAGS) polypeptide to illustrate its different domains (shown to scale; vertical lines mark domains boundaries; residue numbers below the chain). The *conserved domain*, expressed here, is active and regulated by arginine.[34] It is composed of the amino acid kinase-fold domain (AAK) and the GCN5-related *N*-acetyltransferase catalytic domain (GNAT). (B) Scheme of the chimera produced. The masses of the entire chimera, of the truncated chimera lacking the GNAT domain, of the MBP and cHuNAGS moieties, and of the AAK and GNAT domains are given. (C) Coomassie-stained SDS-PAGE gel to illustrate the purification process and the cleavage of the purified protein. *Centrifugation of sonicate*: equal volumes applied of the postcentrifugation *supernatant*, and of the *precipitate* (resuspended in the original volume of extract). *Ni affinity purification*: equal amounts of protein (Bradford assay) from the two 0.2-mL fractions collected with imidazole elution. *Centrifugally desalted*: equal amounts of protein following buffer exchange, prior and after PreScission protease cleavage. Arrowheads identify protein bands in the gel. The specific activities (U/mg) prior to cleavage and after PreScission cleavage are given at the bottom right for the desalted protein. St, protein standards, with corresponding masses (in kDa) indicated to the left. (D) Influence of time of storage at 4°C on enzyme activity of the uncleaved and cleaved sample. The samples were given a fast spin (3 min, top speed, 4°C, Eppendorf microcentrifuge) before assaying the activity in the supernatant. Activity is given relative to the value at zero time. (E) Ratio of activities before and after cleavage in six preparations (individual dots; the bar gives the mean and SD for the six ratios).

data set on firm ground disease causation and mechanisms, having an impact on clinical counseling, and potentially guiding the development of novel therapies.

This study exemplifies with NAGSD the potential for UCDs of in vitro assays with pure recombinant human enzymes.

2 | MATERIALS AND METHODS

2.1 | Cloning of the coding sequence for cHuNAGS in an expression plasmid

The cHuNAGS coding sequence (HuNAGS residues 95–534, Figure 1A) was PCR-amplified with primer pair 2 (Table S1) from a plasmid hosting the coding sequence for mature HuNAGS (HuNAGS residues 50–534[11,12,34]) that had been PCR-cloned from the Megaman Human Transcriptome Library (Stratagene) using primer pair 1 (Table S1). The purified product was ligation-free cloned into HindIII and KpnI-digested pOPINM (Addgene, plasmid no. 26044). The resultant pOPINM-cHuNAGS encodes the His_6-MBP-cHuNAGS chimera, in which the 9-amino acid MBP-cHuNAGS linker LEVLFQGPM (single-letter amino acid code) hosts a cleavage site (at Q/G) for the human rhinovirus 14-3C protease (HRV3C protease; trivial name, PreScission protease). Sanger sequencing corroborated the correctness of the constructions and the absence of unwanted sequence changes (reference sequence, GenBank NM_153006.3; Uniprot KB entry Q8N159).

2.2 | Variants studied and site-directed mutagenesis

For comparative purposes, all the variants studied here (22 amino acid substitutions and a C-terminal truncating mutation that removes the last 37 residues) were found in patients diagnosed of NAGSD. The publications in which they were reported, the patients' genotypes and a summary of their phenotypes are given in Ref. 14 (tables 1 and 2 of Ref. 14). These changes were previously studied with in silico tools and, when feasible, by testing their effects on PaNAGS, used as an imperfect surrogate of HuNAGS.[14]

These substitutions and the truncation, abbreviated in compact single-letter amino acid code (without the p. for protein and the parentheses), are <u>M167V</u>, <u>V173E</u>, <u>C200R</u>, **P260L**, <u>*T264M*</u>, <u>*A279T*</u>, <u>*I291N*</u>, <u>L312P</u>, <u>V350I</u>, *L391R*, S398C, **S410P**, **R414P**, **L430P**, T431I, **E433D**, L442V, **G457D**, **W484R**, **W498Ter** (abbreviated here for brevity as **W498***), R509Q, Y512C, and *A518T*. In this listing, the figures give the amino acid number in the HuNAGS protein sequence. The underlining and nonunderlining indicate that the change respectively maps in the amino acid kinase (AAK) and GCN5-related *N*-acetyltransferase (GNAT) domains of HuNAGS (Figure 1A). Bold and italic types indicate probable causation of, respectively, neonatal and late-onset presentations of NAGSD. Normal type indicates insufficient information for associating the change to neonatal or late-onset presentations.[14]

We generated the variant forms of the chimera for each one of the above 23 changes by site-directed mutagenesis of pOPINM-cHuNAGS, using either the commercial Quickchange System (Stratagene, La Jolla, CA) or the PCR overlap extension method,[35] utilizing the mutagenic primer pairs listed in Table S1 (pairs 3–25). Sanger sequencing corroborated the presence of the desired change and the absence of unwanted changes.

2.3 | Production and purification of the MBP-cHuNAGS chimera (wild-type and variants) and release of cHuNAGS by linker cleavage

Rosetta (DE3) pLysS *E. coli* cells (Novagen-Sigma Aldrich/Merck) transformed with wild-type (WT) or variant forms of pOPINM-cHuNAGS plasmid were grown at 37°C in 20 mL liquid LB medium containing ampicillin (100 μg/mL) and chloramphenicol (35 μg/mL). When the culture attained OD^{600} 0.6–0.8, it was left standing 1 h on ice, and then 0.5 mM isopropyl-β-δ-thiogalactoside was added, followed by overnight culturing at 20°C. Subsequent steps were done at 4°C. After centrifugation, harvested cells were suspended in 1.2 mL of buffer A (20 mM Na phosphate pH 8, 1 mM dithiothreitol [DTT], 0.5 M NaCl, and 20 mM imidazole), sonicated on ice/water and centrifuged (15 000 × g, 20 min), collecting the supernatant and suspending the precipitate in 1.2 mL of buffer A. The MBP-cHuNAGS chimera was purified from the supernatant in a single step using a buffer A-equilibrated 0.1-ml His-Spin-Trap centrifugal column (from Cytiva, Barcelona) according to column instructions. We applied to the column in succession, with intervening centrifugations, the ∼1.2 mL supernatant (two 0.6-mL applications), a 0.6 mL wash, and two applications of 0.2 mL of 0.5 M imidazole-supplemented buffer A, collecting separately the last two effluents, which contained the purified chimera. After buffer exchange using 0.6-mL PD SpinTrap G-25 columns (from Cytiva) equilibrated in conservation solution (10 mM Na phosphate pH 7.0, 15% v/v glycerol, 1 mM EDTA, 1 mM DTT, 20 mM NaCl, and 10 mM NAG; based on[14,36]), the chimera was stored at 4°C.

The linker was cleaved by 3-h incubation at 15°C of a mixture of 90 μL of 0.5 mg/mL of the chimera in conservation solution and 10 μL of 0.4 mg/mL of PreScission protease (His_6-tagged; home preparation) in 0.5 M Tris–HCl pH 7.1, 1.5 M NaCl, 10 mM EDTA, and 10 mM DTT. Completeness of the cleavage was confirmed in all cases by sodium dodecyl sulphate polyacrylamide gel electrophoresis (SDS-PAGE). Assays on the separate cHuNAGS were carried out immediately after PreScission

digestion using as enzyme preparation the cleavage mixture exhibiting complete linker cleavage.

2.4 | Enzyme activity assays

NAGS activity was determined as glutamate-dependent coenzyme A (CoA) release (in 10 min at 37°C) using a modification[14] of the colorimetric method described in Ref. 37 In the standard assay, L-glutamate (Glu; as mono-Na salt) and acetyl-CoA (AcCoA) were at 0.1 M and 6 mM respective concentrations. The enzyme stock solution, diluted in enzyme dilution buffer (10 mM Na-phosphate pH 7.0, 15% v/v glycerol, 1 mM EDTA, 1 mM DTT, 30 mg/mL bovine serum albumin), was added in 10% of the assay volume. When indicated, 1 mM or variable concentrations of L-arginine were added. For substrate kinetics assays, the concentration of AcCoA was kept at 6 mM when Glu was varied; or Glu was kept at 100 mM when AcCoA was varied. Further details are as in Refs. 14. Duplicate tubes were prepared for each assay, and assays were repeated at least twice. Kinetic results were fitted with Prism (GraphPad Software, San Diego) to Michaelis–Menten hyperbolic kinetics. One enzyme unit produces 1 μmol CoA/min (see Refs. 14,37).

Thermal inactivation of enzyme activity was monitored following linker cleavage (unless indicated). The enzyme solution, after cleavage, was diluted 10-fold in dilution buffer at 4°C and divided in 20 μL-aliquots that were heated in parallel for 15 min at the indicated temperatures, followed by cooling in ice-water bath, and immediate enzyme activity determination by using the standard assay at 37°C.

2.5 | Other techniques

Analytical size exclusion chromatography was performed by using a Superdex 200 Increase 5/150 GL column (from Cytiva) equilibrated and run (0.2 mL/min) with a solution at 4°C of 50 mM Tris–HCl pH 8.5/0.1 M NaCl, using the NGC chromatographic system (BioRad), monitoring the effluent optical absorption at 280 nm.

SDS-PAGE used 10% polyacrylamide gels, and pre-stained protein standards for mass comparison (PageRuler, product 26 616 from Thermo Scientific; or BLUltra pre-stained protein ladder, product PM001-0500 from Gene-DireX). Gels were Coomassie stained and their images were digitally scanned. When required, densitometric analysis was performed using the Multi Gauge quantification software from Fuji Film (Fuji Photo Film Co., Tokyo, Japan).

Western blotting after semidry transferring of proteins to nitrocellulose membranes (Amersham Protran

Premium 0.2 NC, from Cytiva) allowed direct His$_6$-tag detection by luminescence (ECL Select System, with capture in an Image Quant LAS4000 apparatus, from Cytiva) using a peroxidase-conjugated mouse Anti-His$_6$ monoclonal antibody (Reference 11 965 085 001 from Roche; used at 1/1000 dilution).

Protein was determined by a Bradford commercial assay (Bio-Rad) using bovine serum albumin as standard.

3 | RESULTS

3.1 | Production of a stable MBP-cHuNAGS chimera and release of the cHuNAGS component

The MBP-cHuNAGS chimera (Figure 1B) was abundantly expressed (Figure 1C, *E. coli* sonicate) in *E. coli* transformed with the pOPINM-cHuNAGS plasmid. It was soluble, being recovered in the supernatant following centrifugation (Figure 1C, compare *Supernatant* and *Precipitate* tracks). It was purified to essential homogeneity by fast Ni-affinity chromatography (Figure 1C, tracks under *Ni affinity purification*). The buffer used for elution of the chimera was exchanged by conservation buffer in a single fast centrifugal desalting step. The purified chimera was enzymatically active (Figure 1C, *Not cleaved* track under *Centrifugally desalted*; enzyme activity given at the track bottom). At 4°C, it remained soluble and active (Figure 1D, *Not cleaved*). The chimera had its linker specifically cleaved by PreScission protease, with total digestion, yielding the separate MBP and cHuNAGS components, with concomitant modest increase of enzyme activity (Figure 1C, *Centrifugally desalted/HRV3C protease-cleaved*; and Figure 1E). However, in the cleaved preparation, separate cHuNAGS aggregated on standing at 4°C, decreasing soluble enzyme activity (Figure 1D, *Cleaved*). Remarkably, although at 4°C the chimera stabilized cHuNAGS, it did not do so at temperatures above 30°C, as shown by the essentially identical profiles of thermal inactivation of the NAGS activity in the intact chimera or following linker cleavage (Figure S1).

Limited attempts to isolate cHuNAGS following linker digestion failed. In these attempts, we used centrifugal Ni-affinity chromatography (not shown) or conventional size exclusion chromatography (Figure S2A). Separate cHuNAGS did not emerge from the corresponding columns, while the separate MBP component did emerge from the size-exclusion column (Figure S2A, red trace, and SDS-PAGE inset showing a 40-kDa St marker). In contrast, prior to linker cleavage, the chimera was eluted from the size-exclusion column, although as a
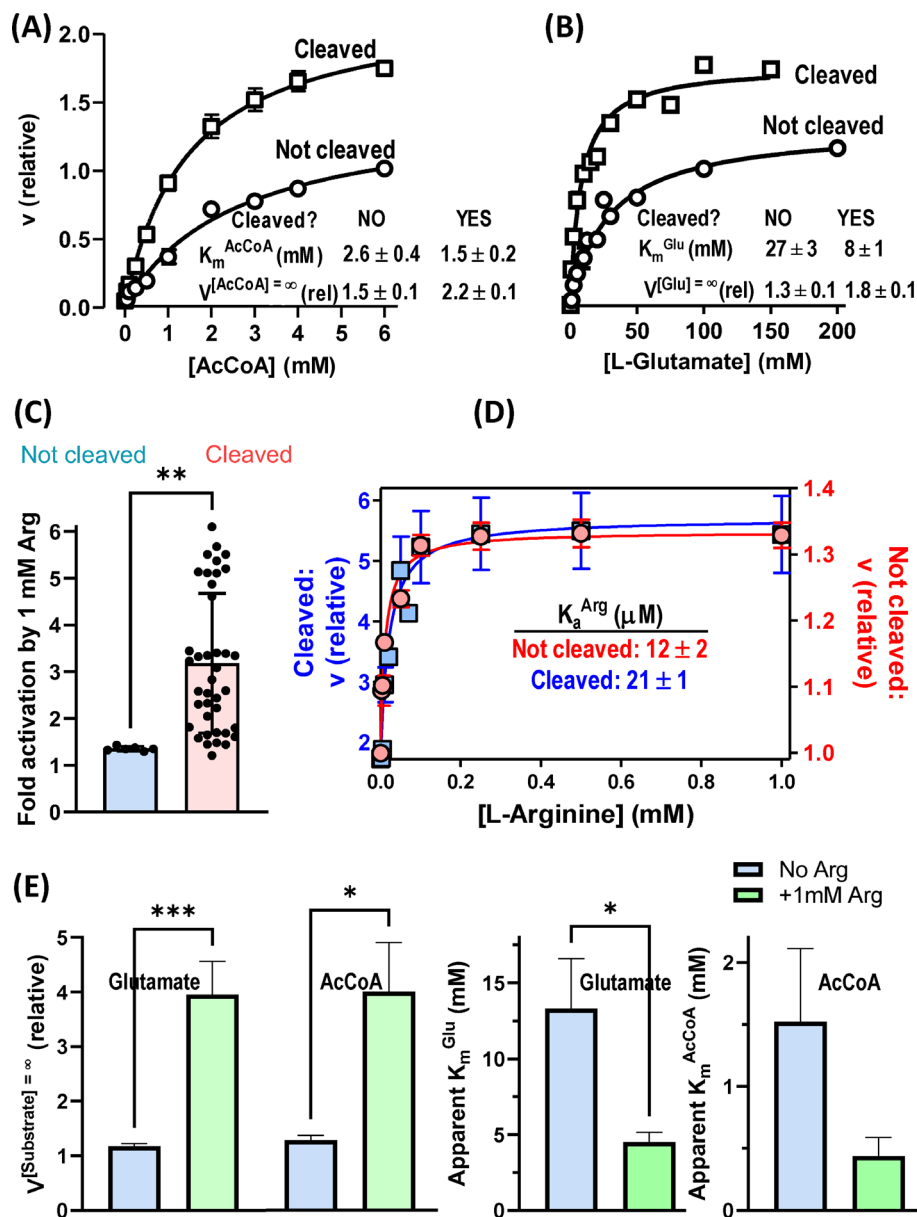
FIGURE 2 Influence of linker cleavage on substrates kinetics for the *N*-acetylglutamate synthase (NAGS) reaction and on arginine activation. (A,B) Substrate kinetics for Acetyl-CoA (AcCoA) (A) and L-glutamate (B). Velocities are expressed in relative units ($1 =$ activity of the non-cleaved chimera in the standard assay; same *y*-axis for both substrates). The curves are hyperbolae. Data and kinetic parameters shown are given as means $\pm$ SE. The number of "not cleaved" and "cleaved" preparations used were, respectively, 3 and 7 for AcCoA and 5 and 9 for Glu. (C) Activation by 1 mM arginine of the not cleaved and linker-cleaved chimera, as indicated. Dots correspond to individual determinations of the quotient $v^{[Arg]=1mM}/v^{[Arg]=0}$. Column heights/error bars, mean/SD. **Statistical significance ($p < 0.005$, unpaired *t*-test). (D) Dependency of NAGS activity in the standard assay on the concentration of arginine, for the linker-cleaved (left *y*-axis; blue-filled squares) and the noncleaved (right *y*-axis; red-filled circles) chimeric protein. The curves are hyperbolae passing by 1/1.8 (noncleaved/cleaved) at [Arg] $= 0$. Data are means $\pm$ SE (four preparations). (E) Effects of 1 mM arginine on substrate kinetics of the NAGS reaction. Values for AcCoA and glutamate are means $\pm$ SE for three (AcCoA) or four (Glu) preparations of linker-cleaved chimera. Velocities are expressed in relative units (as defined in A,B). *** and * denote statistical significance (unpaired *t*-test) with *p*-values of $p = 0.0005$ and $0.01 < p < 0.05$), respectively.

broad early peak (Figure S2A, line in black, and SDS-PAGE inset showing 100 and 70 kDa St markers) suggesting dynamic equilibrium between different oligomeric forms (Figure S2B). Given our inability to isolate pure

cHuNAGS, we tested the effects of single-amino acid variation on the properties of separate cHuNAGS assayed in the unfractionated digestion mixture immediately after termination of the digestion step.

3.2 | Effects of linker cleavage on the kinetics of HuNAGS for its substrates and for arginine activation

Kinetic assays (Figure 2A,B) showed a modest decrease (<3.5-fold) in apparent K_m values for both substrates and ~50% increase in apparent V_{max} (velocity at infinite concentration of Glu or AcCoA) upon linker cleavage. These K_m and V_{max} effects contribute in similar proportions to the activity increase upon linker cleavage. The enzyme activity per mg of separate cHuNAGS (specific activity; the amount of cHuNAGS was quantified densitometrically from Coomassie-stained SDS-PAGE gels, following PreScission digestion), was estimated to be 46.3 ± 1.8 U/mg (mean ± SE, $n = 30$) in the standard assay at 100 mM Glu and 6 mM AcCoA, extrapolating to a V_{max} (infinite concentrations of both substrates) of ~63 U/mg, corresponding to a turnover number of ~52 s^{-1} (assay temperature, 37°C).

Linker cleavage also importantly increased cHuNAGS activation by arginine in the standard assay, from ~40% activation before cleavage, to ~330% mean activation following linker cleavage (Figure 2C). This effect was largely due to increased $V^{[Arg]=\infty}$ rather than to changes in K_a^{Arg}, since the enzyme was saturated by the 1 mM arginine used in the standard assay before and after linker cleavage (Figure 2D). Puzzlingly, the degree of arginine activation varied from 60% to 600% activation in different preparations of the cleaved chimera (Figure 2C). This variability replicates the variable degree of activation by arginine reported for rodent NAGS extracted from liver mitochondria,[38,39] an in vivo variability that remains unexplained.[40] In any case, arginine activated cHuNAGS by increasing apparent V_{max} (Figure 2E, left panel), while also decreasing apparent K_m values for its two substrates (Figure 2E, right panels). These decreases in K_m values might affect more NAGS activity in liver mitochondria than observed in our substrates-rich standard activity assay, since in these organelles substrates may be at subsaturating concentrations (see Section 4). For a mean activation of 330% by 1 mM arginine, taking into account the apparent K_m values for both substrates at 1 mM arginine (Figure 2E), a V_{max} of 225 U/mg can be estimated at saturation of arginine, corresponding to a turnover number of the arginine-activated enzyme of ~185 s^{-1}.

3.3 | Effects of single-amino acid variants on the chimera produced in *E. coli*

We assessed the effects of each one of the 23 changes listed in Section 2.2, individually introduced in the recombinant protein (Figure 3A). The chimera (Figure 3A, band marked with black arrowpoint) was robustly expressed for WT and for all variants and was largely soluble in the initial extract, as shown by its recovery mostly in the supernatant obtained after centrifugation (Figure 3A). Only for the V173E and L312P variants there appeared to be an increase in the fraction of chimera in the precipitate (Figure 3A). As expected from the lack of 37 residues at the C-terminus, the chimera of the **W498*** variant migrated in SDS-PAGE ahead of the other chimeras (Figure 3A).

Purification of the chimera was successful for most variants, as shown by SDS-PAGE analysis of the purified preparations, which showed bands of the chimera of similar intensity and identical migration as for the WT form (Figure 3B, tracks labeled *NC*). Similarly, the purified preparations of most variants yielded upon PreScission digestion (Figure 3B, tracks labeled *C*) the same two bands of separate MBP and cHuNAGS components that were observed with the chimera for WT cHuNAGS. Only for five variants, V173E, *L391R*, **R414P**, **L430P**, and **W498***, the outcome of SDS-PAGE analysis of each purified preparation before and after PreScission digestion was clearly different from that for WT (Figure 3B, see *NC* and *C* tracks for these variants). Among these five variants, the one which hosts the amino acid change in the AAK domain, V173E, had a very low yield of pure chimera before PreScission cleavage, and of the cHuNAGS component after PreScission cleavage (Figure 3B, bands for this variant marked with black arrowheads in the *NC* and *C* tracks), strongly suggesting gross misfolding and degradation for this variant. The other four variants, *L391R*, **R414P**, **L430P**, and **W498***, host amino acid changes in the GNAT domain and showed on SDS-PAGE banding patterns strongly suggestive of selective GNAT domain misfolding and loss. Thus, the normal band of the chimera was faint, being largely replaced by a faster band which migrated identically for the four variants, at the position expected for a chimera of the MBP and just the AAK domain of cHuNAGS (Figures 1B and 3B, NC tracks for these variants, band marked with white arrowhead). The identical migration of this fast band for the **W498*** variant and for the *L391R*, **R414P**, and **L430P** variants (Figure 3B) agrees with the lack of the GNAT domain, since this domain is shorter in the **W498*** variant (lack of the C-terminal 37 residues) and, if it were present, it would have led to an even faster migration of the fast band for this variant. Furthermore, this fast band was immunostained in western blots by anti-His$_6$ antibody (Figure 3C), showing that this reduced-size chimera includes the normal N-terminus, leading to the conclusion that the part missing is C-terminal, as expected for loss of the GNAT domain. Indeed, also as expected, PreScission digestion of the *L391R*, **R414P**, **L430P**, and

FIGURE 3 Legend on next page.

W498* variants resulted in a normal band for the separate MBP component, whereas the band of separate cHuNAGS was much fainter, with appearance of a new faster band migrating as expected for the isolated AAK domain (Figure 3B,C tracks for these variants, band marked with white arrowpoint).

3.4 | Enzyme activity assays support the impact of variant-induced cHuNAGS misfolding

Observation of the SDS-PAGE patterns reveals that the purified preparations of the misfolding variants, V173E, L391R, R414P, L430P, and **W498***, still contain small amounts of the normally sized chimera and, after digestion, of the separate cHuNAGS (Figure 3B, NC and C tracks for these variants). However, these preparations were enzymatically inactive both before and after PreScission digestion (Figure 3D, red and blue lines, respectively). Therefore, for these variants, even the complete chimera and the complete cHuNAGS are essentially inactive. Enzyme inactivation was to be expected if the GNAT domain was grossly misfolded, given the responsibility of this domain in substrate binding and catalysis[41,42] (Figure 1A). Some degree of GNAT domain misfolding might also account for the important decrease in activity observed for the **E433D** and **W484R** GNAT domain variants, and for the less important activity decreases observed for the S398C, **S410P**, and T431I variants (Figure 3D), five variants in which the amino acid

changes map in the GNAT domain. Indeed, SDS-PAGE of these variants also showed a less marked but substantial fast band of the chimera (corresponding to loss of the GNAT domain), and, after PreScission digestion, a fainter cHuNAGS band (Figure 3B). Interestingly, another GNAT domain variant, **G457D**, was totally inactive despite the lack of obvious evidences of misfolding (no fast band of the chimera; no fainting of the cHuNAGS band postdigestion, Figure 3B), strongly suggesting direct affectation of the substrate-binding/catalytic machinery in this variant.

3.5 | Effective activity yield and disease-causation

The yield of pure complete chimera per L of initial culture, estimated after densitometry of Coomassie-stained SDS-PAGE gels, was reduced ∼90% for the V173E, L391R, **L430P**, and **W498*** variants, 75%–80% for the **S410P** and **R414P** variants, and ∼50–75% for the C200R, **P260L**, T264M, I291N, L312P, T431I, **E433D**, L442V, and R509Q variants (Figure 4A). This suggests that, among the 23 variants studied here, these 15 variants negatively affected the partition of the chimera between well-folded and improperly folded forms, with the latter forms being lost during purification.

We determined the activity per mg of pure cHuNAGS (specific activity) for each variant as the quotient of activity after digestion versus the amount of separate cHuNAGS determined densitometrically from SDS-PAGE

FIGURE 3 Impact of *N*-acetylglutamate synthase deficiency (NAGSD) clinical variants on production, solubility, purification, and activity of cHuNAGS. WT, wild-type form of cHuNAGS. St, prestained protein markers. Variant names give the change in protein sequence in single-letter amino acid notation. In (A,B), blue rectangles and italic type denote that the variant is believed to cause neonatal presentation or late-onset presentation, respectively. Horizontal blue and red lines over the variant names indicate the respective amino acid kinase (AAK) or GCN5-related *N*-acetyltransferase (GNAT) domain mapping of the variant. (A) Coomassie-stained SDS-PAGE of precipitate, P, and supernatant, S, collected after centrifugation of the initial crude extracts of *E. coli* expressing the indicated variants of the MBP-cHuNAGS chimera (band marked with a black arrowpoint). (B) Coomassie-stained SDS-PAGE of purified preparations of WT and the cHuNAGS variant chimeras, NC, or after digestion with PreScission protease, (C) For each variant, NC and C are adjacent tracks in the same gel. The standards shown with each variant also are from the same gel, but the track may not be adjacent, what is indicated with the blue vertical lines separating them from the tracks for the variant, which are aligned with the standards exactly as they appear in the gel. In NC tracks, black arrowpoints mark the band of the complete chimera and white arrowpoints mark the band for the chimera lacking the GNAT domain (shown only for five variants). In the C tracks, the black arrowpoint and the black circle mark the bands for the cHuNAGS and MBP moieties, respectively, whereas the white arrowpoint marks the separate AAK domain. (C) Western blot (right panel in black) and immunoperoxidase staining with anti-His₆ (murine monoclonal IgG1 labeled with peroxidase) of the purified WT and variants chimeras. The samples were not digested with PreScission protease. The standards are prestained and shown on the same membrane (superimposition of luminometric and visual images). For comparison (panel to the left), Coomassie-stained SDS-PAGE of an identical gel run in parallel. (D) Enzyme activities (standard assay without arginine, see Section 2) of purified preparations of the indicated chimeras prior to (red) and following (blue) digestion with PreScission protease. The data (U/mg of total protein) are mean ± SE for at least two preparations. The lines connect the mean values of activity (no symbols shown, but error bars are shown) for the different variants. In this panel, the variant names are underlined and not underlined when they map in the AAK and GNAT domains, respectively. They are in bold type, italic type, and normal type when they cause, respectively, neonatal, late onset and uncertain presentations of NAGSD.
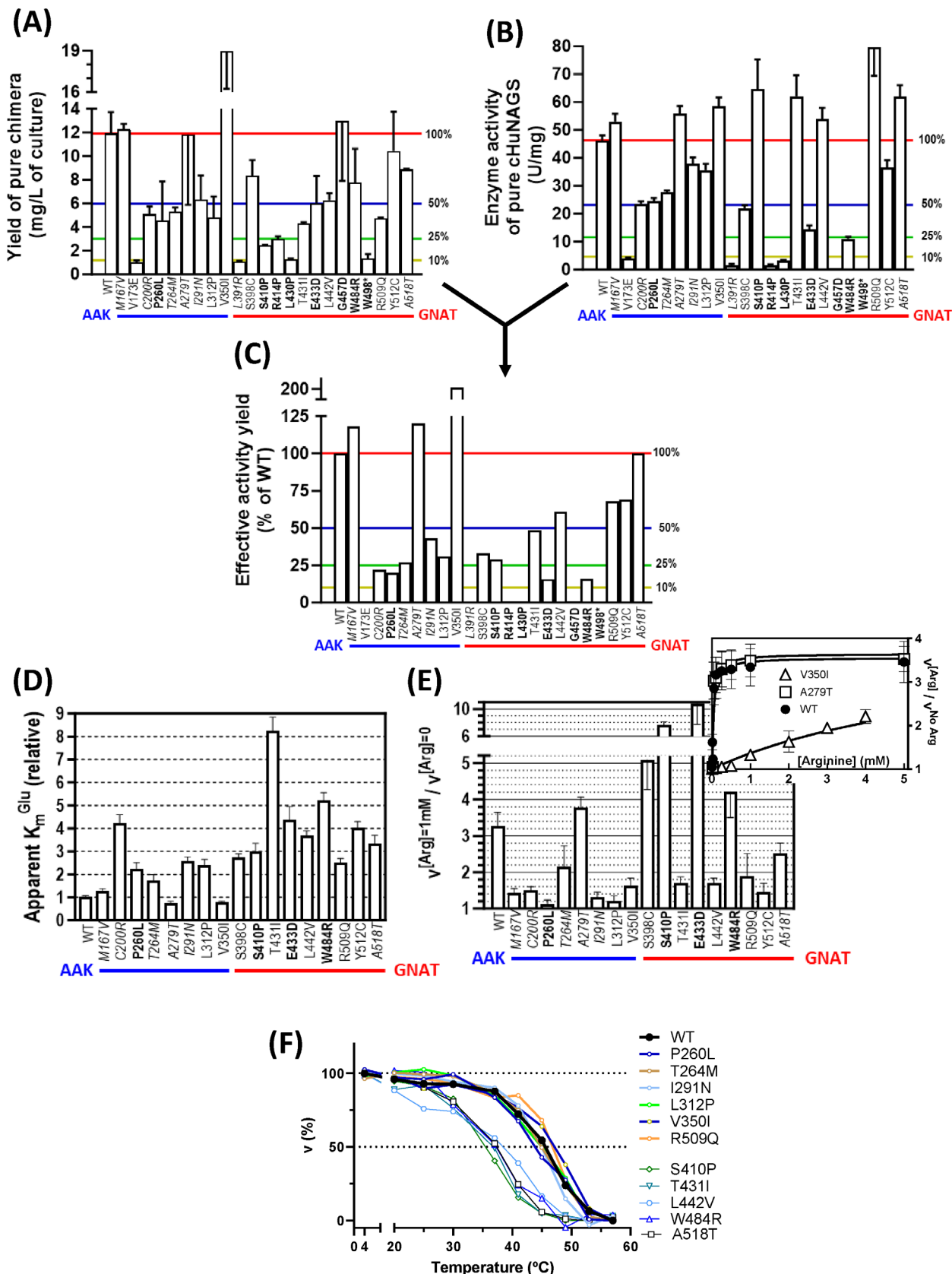
FIGURE 4   Legend on next page.

gels. The specific activity was reduced ≥90% for six variants (V173E, *L391R*, **R414P**, **L430P**, **G457D**, and **W498***), ~75% for two variants (**E433D** and **W484R**) and more modestly (~50%) for four variants (*C200R*, **P260L**, *T264M* and S398C; Figure 4B).

In the liver, the effective activity of a given variant should reflect both the amount of enzyme protein and the specific activity of this enzyme protein. We have tried to approach the relative effective activity of each variant as effective activity yield (EAY). The EAY was estimated for each variant as the product of the mass of pure protein obtained from a fixed volume of culture (given here per L, Figure 4A) times the specific activity of that protein (Figure 4B). We took the EAY for each variant relative to that of WT as an approximation of the relative effective activity of NAGS in liver tissue. Six variants (V173E, *L391R*, **R414P**, **L430P**, **G457D**, and **W498***) decreased ≥99% the EAY, whereas eight variants (*C200R*, **P260L**, *T264M*, L312P, S398C, **S410P**, **E433D**, and **W484R**) decreased it ~70%–85% (Figure 4C). The large magnitude of the decreases in EAY for these 14 variants strongly supports their disease causality.

3.6 | Some variants negatively affect the apparent affinity for glutamate and the arginine activation of NAGS

Mammalian NAGS may not be saturated by its substrates in vivo (see below). Thus, HuNAGS variants that increase K_m values for the substrates should be deleterious. Such kinetic effects may not be recognized in our standard activity assay, since this assay uses high concentrations of the substrates. Therefore, we studied the kinetics for AcCoA for the eight variants presenting ~50% or higher EAY relative to WT (*M167V*, *A279T*, V350I, T431I, L442V, R509Q, Y512C, and *A518T*) without finding among them marked kinetic changes for this substrate (Table S2). In contrast, five of these eight variants, T431I, L442V, R509Q, Y512C, and *A518T*, exhibited substantial increases (range ~3-8-fold; Figure 4D) in the values of the apparent $K_m^{Glutamate}$ (K_m^{Glu}). The magnitude of these increases makes them potentially detrimental for in vivo NAG production, given the glutamate levels (<15 mM) in liver mitochondria.[43] This factor might also contribute to disease causation for other variants, since all the variants mapping in the GNAT domain that had enough activity for kinetic assay presented elevations in the apparent K_m^{Glu} (Figure 4D). This is not surprising, since glutamate is inferred to bind in the GNAT domain.[41,42] Nevertheless, one variant mapping in the AAK domain (*C200R*) also increased importantly (~4-fold) the apparent K_m^{Glu}, further supporting the pathogenicity of this variant.

We also investigated the possibility that the amino acid changes observed could interfere with arginine activation of HuNAGS. Agreeing with the binding of arginine to the AAK domain of NAGS (Figure 1A),[44,45] the *M167V*, *C200R*, **P260L**, *I291N*, L312P, and V350I variants, which map in the AAK domain, strongly decreased or virtually abolished activation of cHuNAGS by 1 mM arginine (Figure 4E). These findings point to hampered arginine activation as a determinant of disease-causation for these variants, supporting the recent conclusion[46] that abolished arginine activation can cause NAGSD. The inset in Figure 4E shows that the affinity for arginine is strongly decreased in the V350I variant, while it

---

FIGURE 4 Impact of *N*-acetylglutamate synthase deficiency (NAGSD) clinical variants on yield (A), specific activity of pure cHuNAGS (B), effective activity yield (EAY) (C), apparent K_m^{Glu} (D), activation by arginine (E), and thermal stability of the enzymatic activity (F). Unless indicated, results are means ± SE for at least two preparations. Blue and red horizontal lines under the names of the variants mark the span of the amino acid kinase (AAK) or GCN5-related *N*-acetyltransferase (GNAT) domains, respectively. Unless indicated, all data (absolute values can be found in Table S2) are for the enzyme after linker cleavage by PreScission protease. (A) Yield of the pure chimera determined as the product of the amount of protein in each homogeneous preparation times the fraction represented by the chimera (determined by densitometry from scans of the Coomassie-stained gels of these purified preparations prior to linker cleavage). (B) Enzyme activity of pure cHuNAGS estimated by dividing the activity in the PreScission protease-digested preparation by the mass of protein represented by the cHuNAGS in that preparation (quantitated by densitometry from Coomassie-stained SDS-PAGE). (C) Effective activity yield of each variant (as a percentage of that estimated for wild-type [WT]). The effective activity yield of a variant is the product of the mean yield of cHuNAGS protein (yield of pure complete chimera multiplied by 0.52 to give the mass corresponding to just cHuNAGS) times the mean value for the specific activity of pure cHuNAGS for that variant. In (A–C), horizontal-colored lines represent 100%, 50%, 25%, and 10% of the mean level for the wild-type form. (D) Apparent K_m^{Glu} for the indicated variants, keeping the concentration of acetyl-CoA (AcCoA) constant at 6 mM. For further details see Section 2. Results are relative to WT which is given a value of 1. (E) Degree of activation of enzymatically active variants by 1 mM arginine. Assays were done in the standard activity assay without and with 1 mM arginine, estimating the ratio between both activities. The inset titrates the effects of different concentrations of arginine for the indicated variants. (F) Illustration of thermal inactivation profiles for WT enzyme and for a number of variants having inactivation profiles highly similar to WT (circles), as well as for the five variants that exhibit significantly decreased stability (noncircular symbols). Each point is the mean of at least four repeated measurements. Horizontal broken lines mark 100% and 50% activity levels.

remained normal for _A279T_, a variant for which no clear molecular derangement was observed. Interestingly, three enzymatically active GNAT domain variants (T431I, L442V, and Y512C) showed hampered arginine activation (Figure 4E), suggesting that these variants impaired transmission of the arginine activating signal from the AAK domain to the catalytic machinery sitting in the GNAT domain.

3.7 | Five variants decrease the thermal stability of cHuNAGS

Similar thermal inactivation profiles of the enzyme activity were observed for WT cHuNAGS and for most variants (Figure 4F). Only for five variants, all of them mapping in the GNAT domain (**S410P**, T431I, L442V, **W484R**, and _A518T_) thermal stability was clearly decreased (Figure 4F), as reflected in the estimated temperature for 50% inactivation (Figure S3). Of note, even for its WT form, cHuNAGS exhibits a temperature of 50% inactivation that is not too far above physiological temperature (Figure S3). Thus, the reduction of ~8–10°C in the temperature of 50% inactivation for these five variants that exhibit significantly reduced thermal stability (Figure S3) may render these variants susceptible of increased inactivation at physiological temperature.

4 | DISCUSSION

The production of stabilized cHuNAGS within a chimera with His_6-MBP has allowed us to examine, after linker cleavage, the properties of HuNAGS without any tag. Here we confirm the observation[47] that tags influence NAGS properties. The similar activities at saturation of both substrates and arginine of our untagged cHuNAGS (225 U/mg at 37°C) and of the best pure preparation of a mammalian NAGS isolated from liver (rat liver, 92.4 U/mg at 25°C),[19] lends support to the use of our untagged cHuNAGS to clarify the effects of patient-identified amino acid variants. This has been done here for 23 changes, encompassing the majority of reported single-amino acid variants in NAGSD, all of them mapping in the conserved domain of NAGS.[13,14]

In this work, hampered NAGS activation by arginine has emerged as a paramount causative factor of NAGSD. A recent study in a NAGS knockout mouse model (koNAGS) proved the physiological importance of arginine activation of NAGS.[46] This was corroborated in an adult-onset human NAGSD patient.[46] This confirmation is generalized here by our finding that 9 of 17 enzymatically active variants (Figure 4B) were not activated or

were poorly activated by arginine (Figure 4E and Table 1). One variant (_M167V_) found to have as sole effect the abolition of arginine activation testifies the severity of lacking arginine activation when the second _NAGS_ allele is null, since this variant was in heterozygosity with a one-base deletion causing a frameshift, in a patient who presented already in the neonatal period with vomiting, poor feeding and episodic confusion.[14] The partial nature of the deficiency due to the abolition of arginine activation is understandable, since the enzyme retains residual activity (the activity and kinetic properties of the nonactivated enzyme). The important increases and decreases in, respectively, apparent V_{max} (Figure 2E, left panels) and K_m values (Figure 2E, right panels) triggered by arginine, and our confirmation[19,47,48] that the K_a^{Arg} (~20 μM here) is much lower than the reported arginine concentrations in liver mitochondria[49,50] further support the physiological importance of arginine activation of NAGS.

Another common derangement observed in patient-found NAGS variants was an increase in apparent K_m^{Glu}, exhibited in 14 of the 17 enzymatically active variants (Figure 4D and Table 1). The range of glutamate concentrations in liver mitochondria (3–15 mM)[43] largely overlaps with the concentration range for this substrate at which NAGS activity is affected, even when the enzyme is saturated with arginine (Figure 2E, right panels). Thus, even modest increases in K_m^{Glu} are likely contributing to cause NAGSD. Although glutamate expectedly binds in the GNAT domain,[41] five changes in the AAK domain increased the apparent K_m^{Glu} (_C200R_, **P260L**, _T264M_, _I291N_, and L312P), suggesting that the AAK domain modulates glutamate binding by the GNAT domain by an allosteric mechanism that would be hampered or abolished by any of these five substitutions. Since four of these AAK domain substitutions (_C200R_, **P260L**, _I291N_, and L312P) also virtually abolish arginine activation, the residues being substituted, Cys200, Pro260, Ile291, and Leu312, may be involved in the transduction of both the constitutive and the arginine-enhanced allosteric signals sent by the AAK domain to the GNAT domain that influence the affinity for glutamate. In turn, three of the GNAT domain variants (T431I, L442V, and Y512C) that increase the apparent K_m^{Glu} also hamper or abolish arginine activation, supporting their involvement in transmitting allosteric signals between both domains of the enzyme.

In contrast with the frequency of hampered NAGS activation or increased K_m^{Glu} found in our study, decreased enzyme thermostability was relatively rare among the enzymatically active variants tested, since it was clearly decreased in only five variants, all of them changes in the GNAT domain. As highlighted in

TABLE 1 Summary of the effects of HuNAGS variants found experimentally in vitro or predicted in silico.

	Variant[a]	Site directed mutagenesis-proven effects on:			In silico predictions		
		Recombinant HuNAGS		Recombinant bacterial NAGS (PaNAGS)[f]	Polyphen-2[g]		Alpha Missense[h]
		This study[b]	Prior studies[c,d,e]				
AAK domain	M167V	No Arg activation	ND	(L50V). No Arg inhibition	ProD	0.931	Ambiguous
	V173E	Strong misfolding. Yield ↓ 90% Specific activity ↓ 90% EAY ↓ 99%	Virtually inactive[c,e]	(L56E). Strong misfolding. Insoluble. 0 yield of pure prot. No activity detected	PosD	0.834	Likely pathog
	C200R	No Arg activation. Yield ↓ 60% Specific activity ↓ 50% EAY ↓ 78%. K_m^{Glu} ↑ 4×	<5% activity[d]	ND	PosD	0.798	Likely pathog
	P260L	No Arg activation. Yield ↓ 60% Specific activity ↓ 50% EAY ↓ 80%. K_m^{Glu} ↑ 2×	ND	(P170L). ↓↓Solubility. ↓Yield Thermal stability ↓15°C	PosD	0.614	Likely pathog
	T264M	Yield ↓ 50% Specific activity ↓ ~50% EAY ↓ 75%. K_m^{Glu} ↑ 1.8×	ND	(S174M). ↓↓Solubility ↓Yield. Vmax↓50%. K_m^{Glu}↑30×. No Arg inhib	PosD	0.893	Likely benign
	A279T	No deletereous effects found	ND	(M189T). ↓Solubility	Benign	0.041	Likely benign
	I291N	No Arg activation. Yield ↓ 50% EAY ↓ ~60%. K_m^{Glu} ↑ 2.5×	ND	(I201N). ↓Solubility. Thermal stability ↓ 20°C	PosD	0.809	Likely pathog
	L312P	No Arg activation. Yield ↓ 60% EAY ↓ 70%. K_m^{Glu} ↑ 2.3×	ND	ND	ProD	0.997	Likely pathog
	V350I	K_a^{Arg} >4 mM and thus, very poor Arg activation	5% activ. No Arg activation[e]	(V258I). ↓Solubility	Benign	0.200	Likely benign
GNAT domain	L391R	Strong misfolding. Yield ↓ 90% Specific activity ↓ 95% EAY ↓ 99%	ND	ND	ProD	0.999	Likely pathog
	S398C	Specific activity ↓ 50% EAY ↓ 70%. K_m^{Glu} ↑ 2.8×	ND	ND	ProD	0.997	Likely benign
	S410P	Yield ↓ 80%. EAY ↓ 70% K_m^{Glu} ↑3 × .Thermal stability↓10°C	<5% activity[d]	ND	ProD	0.964	Likely pathog
	R414P	Misfolding. Yield ↓ 75% Specific activity↓95%. EAY↓99%	ND	ND	ProD	1.000	Likely pathog
	L430P	Strong misfolding. Yield ↓ 90% Specific activity ↓ 95%. EAY↓99%	<5% activity[d]	(L342P). Strong misfolding. Insoluble. ↓↓↓↓Yield. Inactive	ProD	0.999	Likely pathog
	T431I	Poor Arg activation. Yield ↓ 60% K_m^{Glu} ↑ 8×	K_m^{Glu} ↑↑↑[a]	ND	ProD	0.999	Likely pathog

TABLE 1 (Continued)

Variant[a]	Recombinant HuNAGS		Recombinant bacterial NAGS (PaNAGS)[f]	Polyphen-2[g]		Alpha Missense[h]
	This study[b]	Prior studies[c,d,e]				
E433D	Thermal stability ↓ 9°C Yield 50%. Specific activity↓70% K_m^{Glu} ↑ 4×. EAY ↓ 85%	ND	ND	Benign	0.104	Likely pathog
L442V	Poor Arg activation. Yield ↓ 50% K_m^{Glu} ↑ 3.6 × Thermal stability ↓ 7°C	50% activity[e] ↓ Arg activation	(L353V). No deletereous effects observed	ProD	0.997	Likely pathog
G457D	Inactive	ND	(G368D). Inactive ↓Solubility	ProD	0.981	Likely pathog
W484R[i]	Specific activity ↓ 75% K_m^{Glu} ↑ 5×. EAY ↓ 85% Thermal stability ↓ 8°C	<5% activity[d]	(W397R). ↓↓Solubility V_{max} ↓ 90% K_m^{Glu} ↑90×. K_m^{AcCoA}↑45×	ProD	1.000	Likely pathog
W498*	Strong misfolding. Yield ↓ 90% Inactive	ND	ND	–	–	–
R509Q	Yield ↓ 60%. K_m^{Glu} ↑ 2.5×	K_m^{Glu} ↑ 2-fold[c]	ND	ProD	0.999	Ambiguous
Y512C	No Arg activation. K_m^{Glu} ↑ 4×	ND	ND	ProD	1.000	Likely pathog
A518T	K_m^{Glu}↑ ∼3×. Thermal stability↓8°C	<5% activity[d]	ND	ProD	0.998	Likely pathog

Note: GenBank mRNA reference sequence NM_153006.3. Uniprot KB protein reference sequence Q8N159. For the nucleotide changes, the genotypes of patients and families, a summary of clinical data (when available) and reference to the publications originally reporting these variants, see Ref. 14 Unless indicated otherwise, "Yield" refers to pure protein yield in terms of mass; "K_m^{Glu}" refers to apparent K_m^{Glu} value determined in the absence of arginine and at a fixed concentration of 6 mM AcCoA. –, not pertinent since W498* is a nonsense variant found in a patient with a neonatal presentation.[14] Since W498* is a nonsense change mapping in the last exon of the *NAGS* gene, it might also cause mRNA decay.

Abbreviations: AcCoA, acetyl-CoA; HuNAGS, human NAGS; NAGSD, *N*-acetylglutamate synthase deficiency; ND, not done; PaNAGS, *Pseudomonas aeruginosa* NAGS.

[a]Amino acid changes are in compact, single-letter notation. They are inferred from nucleotide sequencing in patients with NAGSD diagnosis.[14] Bold type, italic type, and normal type mark mutations considered in Ref. 14 as causative of, respectively, neonatal, late-onset, or undetermined presentations.

[b]Upwards and downwards-looking arrows indicate increase and decrease, respectively. The data in this column largely summarizes the results of Figure 4 of the present publication. EAY, as defined in Section 3.5; it is given when the decrease on this parameter was ≥50%.

[c]Reported in Ref. 11.

[d]Reported in Ref. 12.

[e]Reported in Ref. 13.

[f]Experiments carried on the NAGS from *Pseudomonas aeruginosa*.[14] The sequence changes that were introduced in PaNAGS[14] are given first, within parentheses, in simplified single amino acid notation. The number of arrows reflects a semiquatitative estimate of the intensity of the effect.

[g]http://genetics.bwh.harvard.edu/pph2/. Accessed on 15 December 2023. The HumVar training set has been used. Scores are from 0 to 1, where the probability of disease causation increases with the value of the score. The diagnostic statements are, from higher to lower probability of being deleterious, Probably Damaging (ProD), Possibly Damaging (PosD) and Benign. For details (see Ref. 55).

[h]AlphaMissense server https://alphamissense.hegelab.org/search asked for variants on human NAGS on 21 December 2023. For shortness, "pathogenic" has been abbreviated to "pathog." For details (see Ref. 16).

[i]At nucleotide sequence level, this variation corresponds[14] to the nucleotide change in the coding sequence c.1450 T > C, which affects the penultimate base of exon 6 at the exon6/intron 6 donor splice site. Thus, it might also affect splicing of exons 6–7, (predicted by MutationTaster2021,[56] https://www.mutationtaster.org/ as "likely to disturb normal splicing").

Section 3.7, cHuNAGS is inactivated even at temperatures occurring in humans during fever (25% inactivation in 15 min at 40°C, Figure 4F). This inactivation could be drastically enhanced in the five enzyme variants in which the temperature of inactivation was strongly decreased (Table 1 and Figure S3) and, therefore, these variants

could decrease product formation in liver tissue by accelerating enzyme inactivation.

Misfolding can be a key negative factor in enzyme deficiencies, and it is potentially treatable with pharmacochaperones (see e.g.,[8]). Five variants in our series (V173E, *L391R*, **R414P**, **L430P**, and **W498***) exhibited clear indications of misfolding. This was manifested for GNAT domain variants as degradative GNAT domain loss (Figure 3B), together with importantly decreased specific activity of residual normal-sized chimera or cHu-NAGS molecules (Figures 3B and 4B and Table 1). Less patent GNAT domain misfolding giving degradative GNAT domain loss was detected in another five GNAT domain variants (S398C, **S410P**, T431I, **E433D**, and **W484R**, see Section 3.4) although among these variants only the **E433D** and **W484R** changes caused a decrease in the specific activity of the complete cHuNAGS molecules (Figure 4B). Two additional GNAT domain-mapping variants, L442V and R509Q, presented somewhat reduced yields of pure chimera (Figure 4A and Table 1) possibly indicating increased tendency to misfold and to be degraded without exhibiting selective GNAT domain degradation. A decrease in the yield of pure chimera was also observed (Figure 4A) for five additional AAK domain variants (C200R, **P260L**, T264M, I291N, and L312P). Overall, 17 of the 23 variants in our series may present at least some increased tendency to misfold, making reasonable to consider NAGSD a misfolding disease.

Total enzyme inactivation was observed only for two changes. One change was **W498***, which eliminates a part of the GNAT domain machinery for substrate binding.[14,41] The other change was the drastic substitution **G457D**, which affects the last residue of the consensus motif [(Arg/Gln)-Xaa-Xaa-Gly-Xaa-(Gly/Ala)] for AcCoA binding among GNATs.[41] In addition to these two variants, the already mentioned V173E, *L391R*, **R414P**, and **L430P** variants exhibited ≥90% decreases in specific activity of cHuNAGS (Figure 4B), actually preventing their kinetic analysis.

The true determinant of deficiency in inborn errors is the effective enzyme activity in the tissue, which reflects both the amount and the specific activity of the enzymatic protein. We have used as a crude approximation to this effective activity, the EAY (Section 3.5), the product of pure protein yield × specific activity of pure cHu-NAGS, expressed as a fraction of the same product for WT cHuNAGS. This estimate does not take into account changes in K_m if these changes are not reflected in the activity in the standard assay. Similarly, it does not reflect possible decreases in arginine sensitivity or in thermal stability. Even with these limitations, we pinpoint 14 variants that decrease EAY by ~70% or more (V173E, C200R,

P260L, T264M, L312P, *L391R*, S398C, **S410P**, **R414P**, **L430P**, **E433D**, **G457D**, **W484R**, and **W498***), accounting for their disease causation. Three of these variants (C200R, **P260L**, and L312P) and six additional variants with non-decreased or less decreased EAY (M167V, I291N, V350I, T431I, L442V, and Y512C) were deficient in arginine activation, a trait that, as already indicated,[46] should also cause partial deficiency. One further variant (A518T) combined a 3-fold increase in K_m^{Glu} with a decrease of 8°C in the temperature of half-inactivation, whereas another variant (R509Q) increased K_m^{Glu} and decreased somewhat EAY (Figure 4C and Table 1), supporting disease causality for both variants. Thus, among the 23 variants examined here, only for one variant (A279T) no disease-causative trait could be found. This variant was observed in homozygosity in an adult patient with a NAGSD phenotype of little severity.[51,52] In prior studies using PaNAGS as surrogate of HuNAGS,[14] we used, in place of the A279T human change, the analogous but non-identical change M189T. This last change partially insolubilized PaNAGS. However, the real change observed in HuNAGSD, A279T, when tested on the genuine human enzyme, did not decrease enzyme solubility and appears not to be detrimental (Table 1).

Our present approach is clearly superior to the one that used PaNAGS as a surrogate of HuNAGS[14] (Table 1). First, the partial sequence conservation of PaNAGS and HuNAGS only permitted testing seven of the present variants, plus four additional substitutions in residues that were conservatively replaced in PaNAGS (M167V, V173E, T264M, and A279T were replaced in PaNAGS by L50V, L56E, S174M, and M189T). In addition, arginine is an inhibitor for bacterial enzymes, and an activator for HuNAGS.[44,45,53,54] Despite these differences, there was essentially complete agreement of the results using PaNAGS[14] and cHuNAGS (present results) for four variants (M167V, V173E, **L430P**, and **G457D**) and partial agreement for another five changes (**P260L**, T264M, A279T, I291N, and **W484R**), highlighting the potential of using surrogate bacterial enzymes when the human enzyme or an animal enzyme is not accessible.

Our findings are also superior to in silico predictions (Table 1). The novel AlphaMisssense[16] labeled as "Ambiguous" the M167V and R509Q changes, and as "Likely benign" the T264M, V350I, and S398C variants. Polyphen 2[55] predictions agreed better with our experimental results, with discrepancy only for the V350I and **E433D** changes, considered benign by that server. Interestingly, both AlphaMissense and Polyphen2, as well as the PaNAGS[14] and the present cHuNAGS experimental systems, were coincident in giving a diagnosis of benignity for the A279T change, supporting the need for reevaluation of the original data and for sequencing of

regulatory regions of the *NAGS* genes of the patient hosting that change.[51,52]

On the basis of informative phenotypes and genotypes, seven and eight of the presently studied variants were considered causative of, respectively, late onset and neonatal presentations, usually equated with less severe and more severe or complete deficiency.[14] These severity labels were closely paralleled by our results for 10 of these variants, and also were compatible for three variants (**S410P**, **E433D**, and **W484R**), while they appeared discrepant with our results for three variants: the already discussed *A279T*, found by us not to cause detectable derangements, and the **P260L** and *L391R* variants, which, from our results, would have been considered causative, respectively, of partial (that is late onset) and complete (neonatal onset) deficiency. The discrepancy for **P260L** may be explained on the basis of potentially severe partial deficiency (combination of low EAY, lack of arginine activation and modest increase of K_m^{Glu} Table 1) that may have given by chance a neonatal presentation in the single patient reported, which hosted this variant in homozygosity.[14] In contrast, our data are totally discrepant with the diagnosis of *L391R* as causative of late onset presentation. This conclusion was inferred[14] from a patient who carried in compound heterozygosity the *L391R* and **W484R** variants and who presented hyperammonemia at month 2 of life that was stabilized with carbamylglutamate, with death after stopping this treatment.[14] The **W484R** variant, which in addition to our findings possibly causes a splicing defect (see footnote of Table 1), was consistently associated in several families with first-week-of-life presentations when in homozygosity.[14] Thus, *L391R*, one of the clear GNAT domain misfolding mutants of the present study, must have exhibited some residual activity in excess of the 1% residual EAY found here. Perhaps the misfolding of this variant cHuNAGS chain is prevented when it associates with the W484R variant chain in hybrid NAGS oligomers, similarly to the stabilization of yeast NAGS when it associates with its homologous enzyme NAG kinase.[20] This possibility would have escaped detection here. In turn, our results for the eight variants for which the patients′ data were non-informative (V173E, L312P, V350I, S398C, T431I, L442V, R509Q, and Y512C) supported for them a diagnosis of partial deficiency, excepting V173E, which should cause in principle complete deficiency because of strong misfolding and very low EAY (Table 1), although the limitation of our assays for misfolding subunits that integrate in hybrid oligomers should be kept in mind.

To conclude, we show for NAGSD the value of testing the effects of the mutations on the protein produced recombinantly, setting on firm grounds the diagnosis of NAGSD, its differentiation from CPS1D, and its treatment with NCG, which, if appropriately dosed, should allow to relieve restrictions of protein intake. Indeed, the information gathered using the recombinant enzyme helps characterize the severity of NAGSD associated to each single amino acid substitution, and can clarify the molecular mechanisms of the deficiency. This last information may also guide novel therapeutic efforts, particularly in developing and utilizing pharmacochaperones.

AUTHOR CONTRIBUTIONS

N.G. carried out experiments, supervised the work of the graduate students B.M.S and B.L.H., analyzed and interpreted the data and participated in the drafting of the article, also revising it critically. E.S-V. participated in the conception of the work and in carrying out the experiments, analyzing and interpreting the data and revising the article critically. M.L.F-M participated in the design of constructs and in the analysis of the data, as well as in the critical revision of the article. B.M.S. and B.L.H. carried out experiments, analyzing and interpreting the data. They also revised the article critically. J.H. participated in the conception of the work, on advising on the genetic and clinical aspects of it and in the critical revision and modification of the article for important intellectual content. C.M-M is the guarantor of the article. She has participated in all the stages of the work, including conception, performing experiments and guiding and supervising the graduate students B.M.S. and B.L.H., analyzing and interpreting the data and participating in the drafting of the article and in revising it critically. V.R. was centrally involved in the conception of the work, in analyzing and interpreting the data and in drafting the article, with strong intellectual involvement on it. All authors have seen the final version of the article, they confirm that the work has not been published/submitted elsewhere and they agree with submission to JIMD.

FUNDING INFORMATION

CONFLICT OF INTEREST STATEMENT

Nadine Gougeard, Enea Sancho-Vaello, María Leonor Fernández-Murga, Borja Martínez-Sinisterra, Badr Loukili-Hassani, Johannes Häberle, Clara Marco-Marín, and Vicente Rubio declare that they have no conflict of interest relative to this work.

DATA AVAILABILITY STATEMENT

All the data are given in the published version and the Supplementary material S1 herein or in the references quoted.

INFORMED CONSENT AND ANIMAL RIGHTS

This article does not contain any studies with human or animal subjects performed by any of the authors. It has used only already published information on anonymous NAGSD patients and thus did not require consent from patients or their legal tutors.

ORCID

Nadine Gougeard https://orcid.org/0000-0001-7338-7267

Enea Sancho-Vaello https://orcid.org/0000-0003-1383-2001

M. Leonor Fernández-Murga https://orcid.org/0000-0001-7123-9834

Johannes Häberle https://orcid.org/0000-0003-0635-091X

Clara Marco-Marín https://orcid.org/0000-0002-8813-3515

Vicente Rubio https://orcid.org/0000-0001-8124-1196

REFERENCES

1. Arranz JA, Riudor E, Marco-Marín C, Rubio V. Estimation of the total number of disease-causing mutations in ornithine transcarbamylase (OTC) deficiency. Value of the OTC structure in predicting a mutation pathogenic potential. *J Inherit Metab Dis*. 2007;30(2):217-226.
2. Kircher M, Kelso J. High-throughput DNA sequencing-concepts and limitations. *Bioessays*. 2010;32:524-536.
3. Gunning AC, Fryer V, Fasham J, et al. Assessing performance of pathogenicity predictors using clinically relevant variant datasets. *J Med Genet*. 2021;58(8):547-555.
4. Gersting SW, Kemter KF, Staudigl M, et al. Loss of function in phenylketonuria is caused by impaired molecular motions and conformational instability. *Am J Hum Genet*. 2008;83(1):5-17.
5. Magini P, Marco-Marín C, Escamilla-Honrubia JM, et al. P5CS expression study in a new family with *ALDH18A1*-associated hereditary spastic paraplegia SPG9. *Ann Clin Transl Neurol*. 2019;6:1533-1540.
6. Tremiño L, Forcada-Nadal A, Rubio V. Insight into vitamin B_6-dependent epilepsy due to *PLPBP* (previously *PROSC*) missense mutations. *Hum Mutat*. 2018;39:1002-1013.
7. Diez-Fernandez C, Martínez AI, Pekkala S, et al. Molecular characterization of carbamoyl-phosphate synthetase (CPS1) deficiency using human recombinant CPS1 as a key tool. *Hum Mutat*. 2013;34(8):1149-1159.
8. Segovia-Falquina C, Vilas A, Leal F, et al. A functional platform for the selection of pathogenic variants of PMM2 amenable to rescue via the use of pharmacological chaperones. *Hum Mutat*. 2022;43(10):1430-1442.
9. Goomber S, Huggins E, Rehder CW, Cohen JL, Bali DS, Kishnani PS. Development of a clinically validated *in vitro* functional assay to assess pathogenicity of novel *GAA* variants in patients with Pompe disease identified via newborn screening. *Front Genet*. 2022;13:1001154.
10. Del Caño-Ochoa F, Ng BG, Rubio-Del-Campo A, et al. Beyond genetics: deciphering the impact of missense variants in CAD deficiency. *J Inherit Metab Dis*. 2023;46(6):1170-1185.
11. Caldovic L, Morizono H, Panglao MG, et al. Late onset N-acetylglutamate synthase deficiency caused by hypomorphic alleles. *Hum Mutat*. 2005;25(3):293-298.
12. Schmidt E, Nuoffer JM, Häberle J, et al. Identification of novel mutations of the human N-acetylglutamate synthase gene and their functional investigation by expression studies. *Biochim Biophys Acta*. 2005;1740(1):54-59.
13. Caldovic L, Morizono H, Tuchman M. Mutations and polymorphisms in the human N-acetylglutamate synthase (NAGS) gene. *Hum Mutat*. 2007;28(8):754-759.
14. Sancho-Vaello E, Marco-Marín C, Gougeard N, et al. Understanding N-acetyl-L-glutamate synthase deficiency: mutational spectrum, impact of clinical mutations on enzyme functionality, and structural considerations. *Hum Mutat*. 2016;37:679-694.
15. Fowler DM, Fields S. Deep mutational scanning: a new style of protein science. *Nat Methods*. 2014;11(8):801-807.
16. Cheng J, Novati G, Pan J, et al. Accurate proteome-wide missense variant effect prediction with AlphaMissense. *Science*. 2023;381(6664):eadg7492.
17. Lo RS, Cromie GA, Tang M, et al. The functional impact of 1,570 individual amino acid substitutions in human OTC. *Am J Hum Genet*. 2023;110(5):863-879.
18. Häberle J, Boddaert N, Burlina A, et al. Suggested guidelines for the diagnosis and management of urea cycle disorders. *Orphanet J Rare Dis*. 2012;7:32.
19. Sonoda T, Tatibana M. Purification of N-acetyl-L-glutamate synthetase from rat liver mitochondria and substrate and activator specificity of the enzyme. *J Biol Chem*. 1983;258(16):9839-9844.
20. Abadjieva A, Pauwels K, Hilven P, Crabeel M. A new yeast metabolon involving at least the two first enzymes of arginine biosynthesis: acetylglutamate synthase activity requires complex formation with acetylglutamate kinase. *J Biol Chem*. 2001;276(46):42869-42880.
21. Shigesada K, Aoyagi K, Tatibana M. Role of acetylglutamate in ureotelism. Variations in acetylglutamate level and its possible significance in control of urea synthesis in mammalian liver. *Eur J Biochem*. 1978;85(2):385-391.
22. Caldovic L, Tuchman M. N-acetylglutamate and its changing role through evolution. *Biochem J*. 2003;372(2):279-290.
23. Hall LM, Metzenberg RL, Cohen PP. Isolation and characterization of a naturally occurring cofactor of carbamyl phosphate biosynthesis. *J Biol Chem*. 1958;230(2):1013-1021.

24. de Cima S, Polo LM, Díez-Fernández C, et al. Structure of human carbamoyl phosphate synthetase: deciphering the on-/off switch of human ureagenesis. *Sci Rep*. 2015;5:16950.

25. Häberle J, Rubio V. Disorders of ammonia detoxification. In: Blau N, Dionisi VC, Ferreira CR, Vianey-Saban C, van Karnebeek CDM, eds. *Physician's Guide to the Diagnosis, Treatment, and Follow-Up of Inherited Metabolic Diseases*. Springer; 2022. doi:10.1007/978-3-030-67727-5_17

26. Kuchler G, Rabier D, Poggi-Travert F, et al. Therapeutic use of carbamylglutamate in the case of carbamoyl-phosphate synthetase deficiency. *J Inherit Metab Dis*. 1996;19(2):220-222.

27. Rubio V, Grisolía S. Treating urea cycle defects. *Nature*. 1981; 292:496.

28. Häberle J, Rubio V. Chapter 19. Disorders of the urea cycle and related enzymes. In: Saudubray JM, Baumgartner MR, García-Cazorla A, Walter JH, eds. *Inborn Metabolic Diseases, Diagnosis and Treatment*. 7th ed. Springer-Verlag GmbH DE, part of Springer Nature; 2022:392-405.

29. Häberle J, Burlina A, Chakrapani A, et al. Suggested guidelines for the diagnosis and management of urea cycle disorders: first revision. *J Inherit Metab Dis*. 2019;42:1192-1230.

30. Yap S, Gougeard N, Hart AR, Barcelona B, Rubio V. N-carbamoylglutamate-responsive carbamoyl phosphate synthetase 1 (CPS1) deficiency: a patient with a novel CPS1 mutation and an experimental study on the mutation's effects. *JIMD Rep*. 2019;48(1):36-44.

31. Gragnaniello V, Gueraldi D, Puma A, et al. Variant in the allosteric domain of CPS1 protein associated with effectiveness of N-carbamoyl glutamate therapy in neonatal onset CPS1 deficiency. *J Pediatr Endocrinol Metab*. 2023;36(9):873-878.

32. Díez-Fernández C, Hu L, Cervera J, Häberle J, Rubio V. Understanding carbamoyl phosphate synthetase (CPS1) deficiency by using the recombinantly purified human enzyme: effects of CPS1 mutations that concentrate in a central domain of unknown function. *Mol Genet Metab*. 2014;112(2):123-132.

33. Díez-Fernández C, Gallego J, Häberle J, Cervera J, Rubio V. The study of carbamoyl phosphate synthetase 1 deficiency sheds light on the mechanism for switching on/off the urea cycle. *J Genet Genomics*. 2015;42(5):249-260.

34. Caldovic L, Morizono H, Gracia Panglao M, et al. Cloning and expression of the human N-acetylglutamate synthase gene. *Biochem Biophys Res Commun*. 2002;299(4):581-586.

35. Ho SN, Hunt HD, Horton RM, Pullen JK, Pease LR. Site-directed mutagenesis by overlap extension using the polymerase chain reaction. *Gene*. 1989;77(1):51-59.

36. Marvil DK, Leisinger T. N-acetylglutamate synthase of Escherichia coli: purification, characterization, and molecular properties. *J Biol Chem*. 1977;252(10):3295-3303.

37. Errey JC, Blanchard JS. Functional characterization of a novel ArgA from *Mycobacterium tuberculosis*. *J Bacteriol*. 2005;187(9): 3039-3044.

38. Shigesada K, Tatibana M. N-acetylglutamate synthetase from rat-liver mitochondria. Partial purification and catalytic properties. *Eur J Biochem*. 1978;84:285-291.

39. Kawamoto S, Ishida H, Mori M, Tatibana M. Regulation of N-acetylglutamate synthetase in mouse liver. Postprandial changes in sensitivity to activation by arginine. *Eur J Biochem*. 1982;123(3):637-641.

40. Kawamoto S, Tatibana M. Arginine activation of N-acetylglutamate synthetase in mouse liver. Enhancement of the sensitivity in vivo by parenteral treatment with inhibitors of nucleic acid and protein synthesis. *FEBS Lett*. 1983;151(1): 117-121.

41. Zhao G, Jin Z, Allewell NM, Tuchman M, Shi D. Crystal structure of the N-acetyltransferase domain of human N-acetyl-L-glutamate synthase in complex with N-acetyl-L-glutamate provides insights into its catalytic and regulatory mechanisms. *PLoS One*. 2013;8(7):e70369.

42. Shi D, Sagar V, Jin Z, et al. The crystal structure of N-acetyl-L-glutamate synthase from *Neisseria gonorrhoeae* provides insights into mechanisms of catalysis and regulation. *J Biol Chem*. 2008;283:7176-7184.

43. Siess EA, Brocks DG, Lattke HK, Wieland OH. Effect of glucagon on metabolite compartmentation in isolated rat liver cells during gluconeogenesis from lactate. *Biochem J*. 1977;166(2): 225-235.

44. Sancho-Vaello E, Fernández-Murga ML, Rubio V. Site-directed mutagenesis studies of acetylglutamate synthase delineate the site for the arginine inhibitor. *FEBS Lett*. 2008;582(7):1081-1086.

45. Min L, Jin Z, Caldovic L, et al. Mechanism of allosteric inhibition of N-acetyl-L-glutamate synthase by L-arginine. *J Biol Chem*. 2009;284(8):4873-4880.

46. Sonaimuthu P, Senkevitch E, Haskins N, et al. Gene delivery corrects N-acetylglutamate synthase deficiency and enables insights in the physiological impact of L-arginine activation of N-acetylglutamate synthase. *Sci Rep*. 2021;11(1):3580.

47. Caldovic L, Lopez GY, Haskins N, et al. Biochemical properties of recombinant human and mouse N-acetylglutamate synthase. *Mol Genet Metab*. 2006;87(3):226-232.

48. Bachmann C, Krähenbühl S, Colombo JP. Purification and properties of acetyl-CoA:L-glutamate N-acetyltransferase from human liver. *Biochem J*. 1982;205(1):123-127.

49. Freedland RA, Meijer AJ, Tager JM. Nutritional influences on the distribution of the urea cycle: intermediates in isolated hepatocytes. *Fed Proc*. 1985;44(8):2453-2457.

50. Horyn O, Luhovyy B, Lazarow A, et al. Biosynthesis of agmatine in isolated mitochondria and perfused rat liver: studies with ^{15}N-labelled arginine. *Biochem J*. 2005;388:419-425.

51. Plecko B, Erwa W, Wermuth B. Partial N-acetylglutamate synthetase deficiency in a 13-year-old girl: diagnosis and response to treatment with N-carbamylglutamate. *Eur J Pediatr*. 1998; 157(12):996-998.

52. Häberle J, Schmidt E, Pauli S, et al. Mutation analysis in patients with N-acetylglutamate synthase deficiency. *Hum Mutat*. 2003;21(6):593-597.

53. Haskins N, Panglao M, Qu Q, et al. Inversion of allosteric effect of arginine on N-acetylglutamate synthase, a molecular marker for evolution of tetrapods. *BMC Biochem*. 2008;9:24.

54. Sancho-Vaello E, Fernández-Murga ML, Rubio V. Mechanism of arginine regulation of acetylglutamate synthase, the first enzyme of arginine synthesis. *FEBS Lett*. 2009; 583(1):202-206.

55. Adzhubei IA, Schmidt S, Peshkin L, et al. A method and server for predicting damaging missense mutations. *Nat Methods*. 2010;7(4):248-249.

56. Steinhaus R, Proft S, Schuelke M, Cooper DN, Schwarz JM, Seelow D. MutationTaster2021. *Nucleic Acids Res.* 2021;49: W446-W451.

SUPPORTING INFORMATION

Additional supporting information can be found online in the Supporting Information section at the end of this article.